FINITE ELEMENT ANALYSIS ON THE BEHAVIOR OF SLAB-COLUMN CONNECTIONS USING PVA-ECC MATERIAL

Asdam Tambusay[a]*, Priyo Suprobo[a], Faimun[a], Arwin Amiruddin[b]

[a]Department of Civil Engineering, Sepuluh Nopember Institute of Technology, Surabaya, Indonesia
[b]Department of Civil Engineering, Hasanuddin University, Makassar, Indonesia
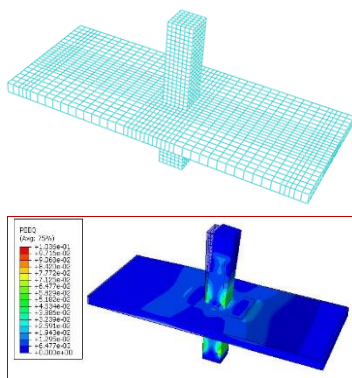
*Corresponding author
asdam.tambusay13@mhs.ce.its.ac.id

Graphical abstract

Abstract

A 3D finite element analysis was carried out to study the behavior of slab-column connections in a flat slab structure under combined gravity and cyclic lateral load. Prior to simulating the behavior of the proposed model, the slab-column connection specimen by using standard orthogonal stud rail from the previous study was modeled with the purpose of verifying the results using finite element tool. Given that numerical simulation was undertaken using ABAQUS to predict the structural behavior of the above-mentioned structure. With regard to providing an accurate result, a sensitivity analysis was performed by changing different parameters, such as dilation angle, viscosity parameter, and damage parameter-strain on both in tension and compression. After gaining the close resemblance to the previous study, the proposed models were then simulated using the similar technique. In the proposed model, drop panel element was used as a replacement of stud rail. Additionally, the engineered cementitious composite material using polyvinyl alcohol fibers (PVA-ECC) was also employed due to its strain capacity of 3-5% under tension compared to 0.01% of conventional concrete. Through this study, the results showed that the effect of utilizing the PVA-ECC material could significantly improve the specimen behavior and damage tolerance.

Keywords: Finite element analysis, ABAQUS, flat slab, slab-column connections, engineered cementitious composite material

1.0 INTRODUCTION

Flat slab structure is one of the structural systems that offers advantages in terms of economy for the possibility to reduce the story height; thus it provides an opportunity to increase the number of floors in the area with strict height restriction [1]. However, due to the absence of beam elements, flat slab structure exhibits low initial stiffness, significant stiffness degradation which can affect the significant strength degradation, and poor energy dissipation under earthquake excitation [2]. Hence, the progressive collapse may occur when the structure is subjected to

major earthquake [3]. In addition, the effect of gravity load in the form of gravity shear ratio (GSR) is a major cause that can deteriorate the behavior of slab-column connection to withstand the lateral load. Therefore, flat slab structure is not appropriate to be applied as primary elements to sustain lateral load [4].

Numerous collapses on flat slab structure have been reported and investigated by several researchers. The failure occurred in flat slab structures, was indicated as brittle punching shear failures when subjected to seismic load [1]. Incidents of structural collapses which took place at Commonwealth Avenue, Massachusetts in 1971 [5], Sempong Department

Store, South Korea in 1995 [6], and also 91 waffle- and flat slab buildings in Mexico City 1995 [7] indicated the failure at slab-column connection due to punching shear.

To ensure the resistance of the structure, several studies related to the improvement behavior on the slab-column connections have been carried out using drop panel [8], shear reinforcement [1, 7], stud rail [2], the post-tensioned system [9], and steel fiber [10]. The use of stud rail as shear reinforcement in a slab-column connection is assessed offering the better result compared with other systems. However, the employment of current stud rail has not completely overcome the structural weaknesses to sustain the combined gravity and seismic load. The use of drop panel as local thickening to prevent the punching failure is also considered did not improve the ductility, which is an essential requirement of earthquake-resistant structures [7].

The engineered cementitious composite (ECC) material which addresses a unique class of high-performance fiber-reinforced concrete with high tensile ductility [11] is proposed in this paper. A particular type of cement-based material is suggested herein to improve the behavior of slab-column connection. Design requirement for this material is based on the experimental investigation employing volume fraction of 2% from polyvinyl alcohol (PVA) fibers. PVA fibers have been used to improve the toughness of quasi-brittle cement-based material [12]. In addition, PVA-ECC is originally designed using the micromechanical concept to create the excessive tensile strain capacity of more than 2% through multiple micro-cracking [13]. In reality, there have been extensive studies to exploit the performance of this material; however, as of today, the application of this material still has not yet been used in the flat slab structure.

Considering all the above, this paper presents the use of PVA-ECC material to upgrade the performance of slab-column connection when being subjected to combined constant gravity and cyclic lateral load. The underlying reason is basically driven due to the fact of brittle punching failure encountered in the flat slab structure can strongly lead to progressive collapse. Therefore, it is a necessity to propose such material that can alleviate the tendency of structure to undergo the brittle response. In this present work, the response of slab-column connection using the above-mentioned material is assessed through the implementation of finite element tool using ABAQUS. It is of interest to use this technique as it offers the possibility to study a larger number of cases than that of experimental test with inexpensive cost and preparation time. Through the modeling process, the suggested alternative to improve the behavior of model as obtained in this analysis is justified by results of numerical modeling.

2.0 METHODOLOGY

2.1 Description of Model Structure

The experimental work by Gunadi *et al.* [14] is briefly explained in this paper to give the detail of specimen being used in the finite element model. The specimen was a half-scale model of isolated interior slab-column connection. The finite element model was based on the sub assemblage system from 3D frame structure with the dual system.

The use of standard/orthogonal stud rail as specified in [15, 16] was utilized in this study to improve the performance of slab-column connection due to the combined gravity and cyclic lateral loading. Gravity loads were given as constant loads from self-weight, superimposed dead load, and reduced live load. The cyclic lateral load which represented the earthquake excitation was given in the form of displacement control at the top of the column. The experimental testing of the model was loaded up to failure by punching.

The dimensions of the specimen are presented in Figure 1. To represent the inflection points in the midspan of prototype slab, roller support was placed at both slab ends of the slab-column connection. Additionally, pin support was also given at the bottom of the column to represent the inflection points occurred in the prototype column. The longitudinal top-bottom flexural reinforcements of the slab (Figure 2), the longitudinal reinforcements of the column, and stirrup of the column (Figure 3) were also prepared.

The concrete cover of column and top-bottom of the plate was 20 mm. The space of column stirrup was designed with a distance of 50 mm. Detail of stud rails used in this study was designed to comply with [15, 16]. Two pairs of stud rails were placed with a distance of 38 mm from column face and embedded (in bottom-up and top-down positions) within the slab using space of 40 mm and interconnected each other using strip plates.
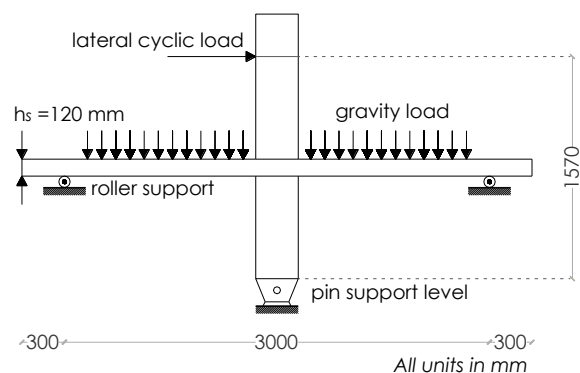

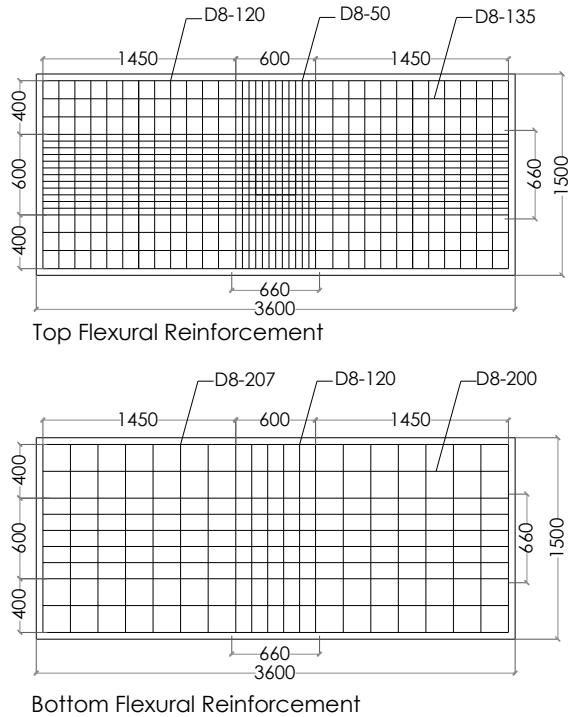**Figure 1** Geometry of specimen by Gunadi *et al.* [14]

Top Flexural Reinforcement

Bottom Flexural Reinforcement

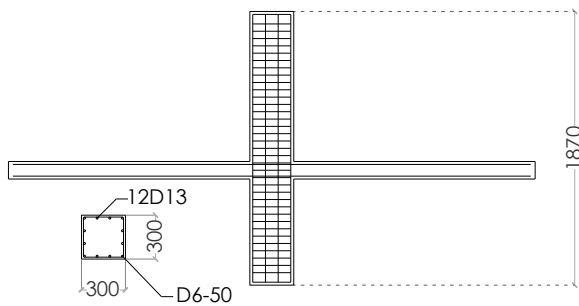**Figure 2** Slab reinforcement layouts by Gunadi *et al.* [14]

Figure 3 Column rebar layouts by Gunadi *et al.* [14]

2.2 Material Properties

The materials used in the experimental work are listed in Table 1.

Table 1 Material test results by Gunadi *et al.* [14]

Designation	Diameter (mm)	Strength (MPa)
Concrete		46.21
Longitudinal bar of column	13.84	390.74
Flexural rebar of slab	7.96	321.5
Column Stirrup	5.94	354.77
Stem	7.68	534.3

2.3 Experimental Procedures

The setup process of the specimen was preceded with the transfer of specimen from pouring location into loading frame by using an overhead crane. Subsequently, pin support at the bottom of the column was fitted followed by the placement of hydraulic actuator at the top of the column before roller support and gravity load were given to structure. In this condition, the balance of specimen was maintained by pin support and actuator. Furthermore, gravity load was applied to the surface of slab followed by the placement of roller support at slab ends.

The gravity load was given in the form concrete blocks of $35 \times 20 \times 28$ cm on the surface of the slab in order to obtain the effect of gravity shear ratio on the behavior of slab-column connection. The cyclic loading process was then performed using displacement control which the drift increased as the cycle increased. Testing of the specimen was stopped after the hydraulic actuator reached its maximum stroke capacity.

2.4 Parameters in Numerical Modeling

A 3D finite element analysis using ABAQUS was implemented in this study. The procedure of modeling was based on experimental work conducted by Gunadi *et al.* [14]. The concrete damaged plasticity (CDP) model was selected to simulate the concrete material behavior by implementing C3D8R brick element. The unit of C3D8R is a kind of three-dimensional solid elements that have eight nodes and is used for calculation about distorted aspect. In addition to the concrete element, normal plasticity using T3D2 truss element was also preferred for reinforcing bars. Using T3D2, it means the reinforcing bars are in the form of steel wire with two degrees of freedom at each node. To create the perfect bond between concrete and reinforcing bars, the embedded constraint was selected. Aside from the aforesaid parameters, the mesh of solid slab-column connection model strictly was constructed following the geometry of the test specimen. To create the mesh of the model, moderately fine mesh at the critical perimeter was given to attain the close response to the experimental results. Figure 4 illustrates the mesh pattern of model structure.
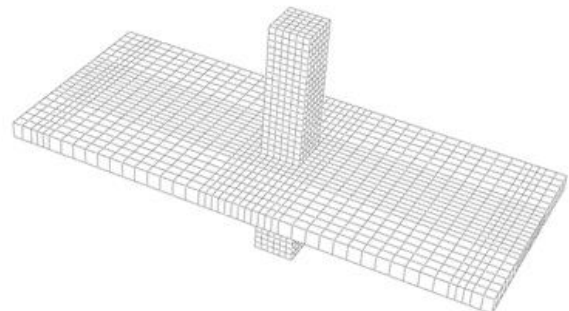

Figure 4 Mesh configuration of numerical model

Concrete damaged plasticity (CDP) model in ABAQUS was implemented to describe the concrete behavior. CDP model, which consisted of plasticity, compressive and tensile properties, input separately. To ensure the stiffness degradation occurs in the numerical model, both of compression and tensile damage parameters were adopted.

The material data used in this study was based on the experimental work as aforementioned. Modulus of elasticity E_{cm} = 35.26 GPa was put as attained from concrete strength of f_{cm} = 46.21 MPa. The strength of concrete was needed to define the analytical compressive stress-strain response as formulated in Eq. (1) [17].

$$\sigma_C = f_{cm} \frac{k\eta - \eta^2}{1 + (k-2)\eta}, \ \ \eta \leq \varepsilon_{cu1}/\varepsilon_C \tag{1}$$

$$\varepsilon_{c1} = 0.0014 \left[2 - \exp(-0.024 f_{cm}) - \exp(-0.14 f_{cm}) \right] \tag{2}$$

where $\eta = \varepsilon_c/\varepsilon_{c1}$, and $k = 1.05\varepsilon_{c1}E_{cm}/f_{cm}$ are defined based on Euro code EC2 concerning the design of concrete. The strain at peak stress as expressed in Eq. (2) [18], nominal ultimate strain ε_{cu1} = 0.0035 [17] for compressive strength. Nevertheless, the stress-strain response of compressive behavior [17] is defined only up to the nominal ultimate strain. As a matter of fact, while also considering concrete strain only up to ε_{cu1}, it can be said that the unreal overestimation of concrete crushing strength may occur [19]. Therefore, compressive stress-strain curve (Figure 6) is extended by Eq. (3) using sinusoidal part between points *D-E* and the linear part between points *E-F* to surpass its nominal ultimate strain [19].

$$\sigma_C = \begin{cases} f_{cm}\left[\dfrac{1}{\beta} - \dfrac{\sin\left(\mu^{\alpha_{tD}} \cdot \alpha_{tE}\pi/2\right) + \mu}{\beta \cdot \sin(\alpha_{tE}\pi/2)} + \dfrac{\mu}{\alpha} \right], \ , \varepsilon_{CuD} < \varepsilon_C \leq \varepsilon_{CuE} \\ \left[f_{CuE}(\varepsilon_{CuF} - \varepsilon_C) + f_{CuF}(\varepsilon_C - \varepsilon_{CuE}) \right]/(\varepsilon_{CuF} - \varepsilon_{CuE}), \varepsilon_C > \varepsilon_{CuE} \end{cases} \tag{3}$$

The tensile stress-strain response is defined as the function of cracking strain and tensile stress. The tensile stress increases linearly up to the peak value of f_{ct}. The proper relation of the tensile stress-strain curve was proposed by Wang and Hsu [20] as can be seen in Eq. (4).

$$\sigma_t = f_{ct}\left(\frac{\varepsilon_{cr}}{\varepsilon_t} \right), \ \ \varepsilon_t > \varepsilon_{cr} \tag{4}$$

Plasticity parameter: biaxial/uniaxial compressive strength ratio σ_{b0}/σ_{c0} = 1.16, flow potential eccentricity ε = 0.1, and deviatoric stress invariant ratio K = 0.667 were given as recommended by ABAQUS [21]. Dilation angle of ψ = 5° was iteratively calibrated to match the experimental test results. Viscosity parameter of v = 0.1 was also iteratively assumed to meet the similar result as experimental work.

As can be seen in Figure 6, damage variable for both of compression and tension were also

considered. The damage parameter is defined as the ratio between undamaged and damaged concrete response with the following formula $d_c = 1 - f_{cm}/\sigma_c$ and $d_t = 1 - f_{ct}/\sigma_t$ for compression and tension, respectively, as a function of inelastic strain. Damage parameters were set to define the stiffness degradation due to service load. If damage parameters are not specified, the model behaves as a plasticity model.

In addition to the stress-strain response of normal concrete, PVA-ECC material was also incorporated using CDP model. For compression, the input parameters of PVA-ECC material was set similar to conventional concrete since their compressive properties are not significantly different to one and another. This also has been stated in the prior studies where the compressive characteristic only has slight discrepancy from normal concrete [23]. Therefore, the equations of conventional concrete can be used to simulate the compressive stress-strain for PVA-ECC material. Regardless of compressive properties, nevertheless, it should be noted that the tensile response of ECC is highly different with normal concrete due to its performance to deliver the excessive tensile strain capacity around 3 to 5%. Given that the equation of tensile stress-strain in conventional concrete cannot be adopted. To deal with ECC, the material investigation incorporating the uniaxial direct tensile test must be undertaken to find out the stress-strain response. However, there has been extensive research carried out to obtain such response. Considering this fact, the results from the previous study can be adapted to initially explore the influence of having such enormous tensile strain when being applied to the structural member. From what is encountered with regard to the past research, the tensile characteristic of PVA-ECC, in general, consist of three distinct features, including linear elastic behavior ε_{t0}, strain hardening behavior associated with multiple micro-cracking until ε_{tp}, and softening behavior prior to failure [23]. Figure 6 also presents the typical idealized tensile stress-strain response parameter for PVA-ECC material.
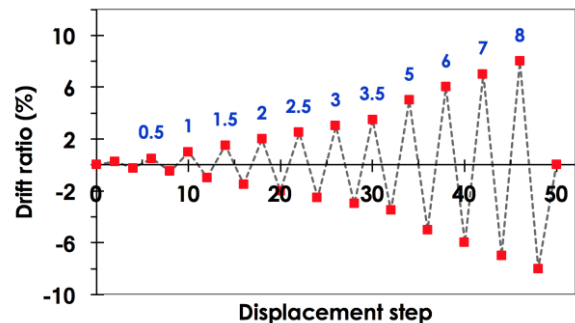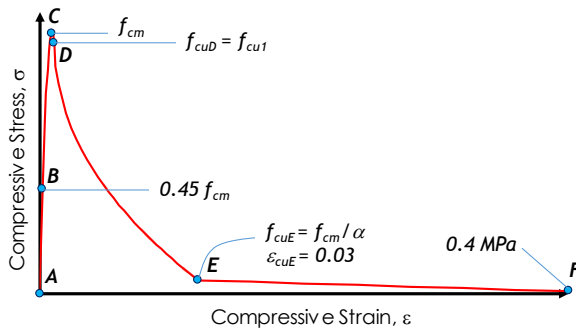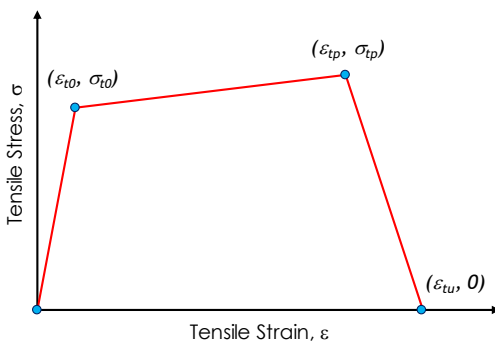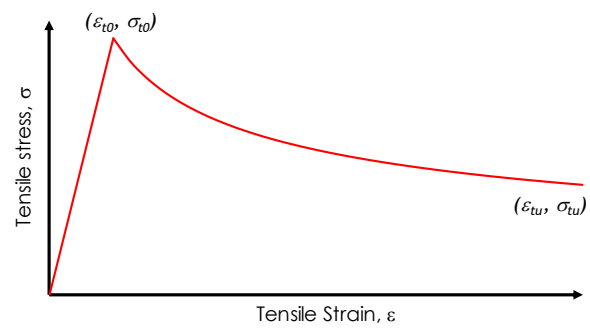

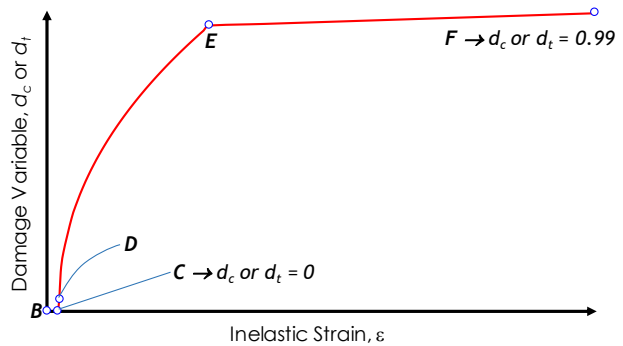**Figure 5** Pattern of lateral cyclic load

Compressive behavior for concrete [19]

Tensile behavior for concrete [18]

Tensile stress-strain for PVA-ECC material [23]

Typical damaged parameter for concrete [19]

Figure 6 Parameters of concrete constitutive model

2.5 Description of Proposed Model

All specimens were half-scale models of interior slab-column connection which designed using the similar materials, dimension and reinforcement details as experimental work. However, in this study, stud rail was removed and replaced with drop panel of 1000 x 600 x 60 mm. PVA-ECC material, on the other hand, was given to specimens at the certain location. A constant 10% of the nominal axial load at the top of the column was also given in each specimen. Detail of each specimen as follows:

(a) *Specimen 1* – flat slab using drop panel with whole conventional concrete.
(b) *Specimen 2* – flat slab using PVA-ECC material only at drop panel
(c) *Specimen 3* – flat slab using drop panel with whole PVA-ECC material

2.6 Gravity Load and Cyclic Lateral Load

By referring to experimental work, gravity load used in this analysis consisted of self-weight, superimposed dead load, and reduced live load. In ABAQUS, self-weight of the model was defined in material properties as density, while other loads were placed on the surface of the slab as applied in experimental work. The total value of superimposed dead load and reduced live load was 2.89 kN/m^2. Gravity load in the form of self-weight was applied to the model by introducing gravitational acceleration g = 9800 mm/sec^2 during linear static response step. After that, the cyclic lateral load was created in the following step.

The cyclic lateral load was performed by referring to [22]. The pattern of the cyclic lateral load is shown in Figure 5. To ensure that drift ratio at the initial step of the test is in the linear condition, the value of moment at slab which causes the first yield stress at flexural reinforcement of slab must be calculated.

2.7 Boundary Conditions

Boundary conditions were modeled by entering data in terms of degree of freedom at the nodal point which coincided with the location of pin support at the bottom of the column. Nodal points were restrained on the axis of X, Y, and Z to represent pin support. Furthermore, nodal points were also restrained at slab ends to represent the roller support as experimental work. Restraints were given on the axis of Y and Z.

3.0 RESULTS AND DISCUSSION

3.1 Verification of Experimental Work

Before performing the proposed FE models in ABAQUS, the model of experimental work by Gunadi *et al.* 14] should be verified numerically. It was carried out to ensure that numerical modeling was based on the appropriate materials, elements, and other parameters.

Several analyses had been executed by changing different parameters, such as dilation angle, viscosity parameter, and damage parameter-strain on both of tension and compression to choose the best performing FE analysis model compared with the experimental work. Figure 7 presents a comparison of backbone curves obtained from the experimental work and numerical modeling.
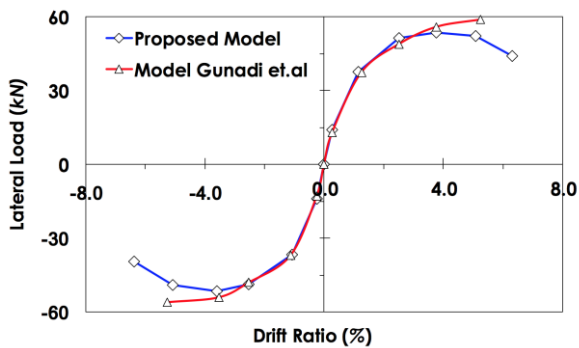

Figure 7 Verified backbone curve of experimental work

As a result of experimental work and numerical study, both of the backbone curves show the similar trend up to drift ratio of 3.5% and slightly different in the following drift ratio. However, it can be said that the numerical modeling has run based on the appropriate techniques. Therefore, further analysis related to the proposed FE model can be carried out.

3.2 Hysteresis Behavior

Hysteresis curves and backbone curves of all specimens are illustrated in Figure 8 and Figure 9. The figures show graphically that all specimens exhibited nonlinear behavior. These figures also imply that the specimen 3 indicates the significant improvement behavior related to the lateral load capacity and strength degradation.

Table 2 shows the value of peak lateral load of each specimen and the strength improvement ratio compared to specimen control. Peak lateral load of specimen 3 is measured at 5.9% of drift ratio which exceeds the required drift ratio of 3.5% [22]. On the other hand, specimen 1 and 2 exhibit the almost similar behavior where the peak lateral load of specimen 1 and 2 have reached the drift ratio of 2.44% and 2.93%, respectively. It can be said that specimen 1 and 2 do not deliver the minimum peak lateral load at the drift ratio of 3.5%. Hence, the feasibility of strength degradation of both of the specimens must be taken into account by following the provision [22].
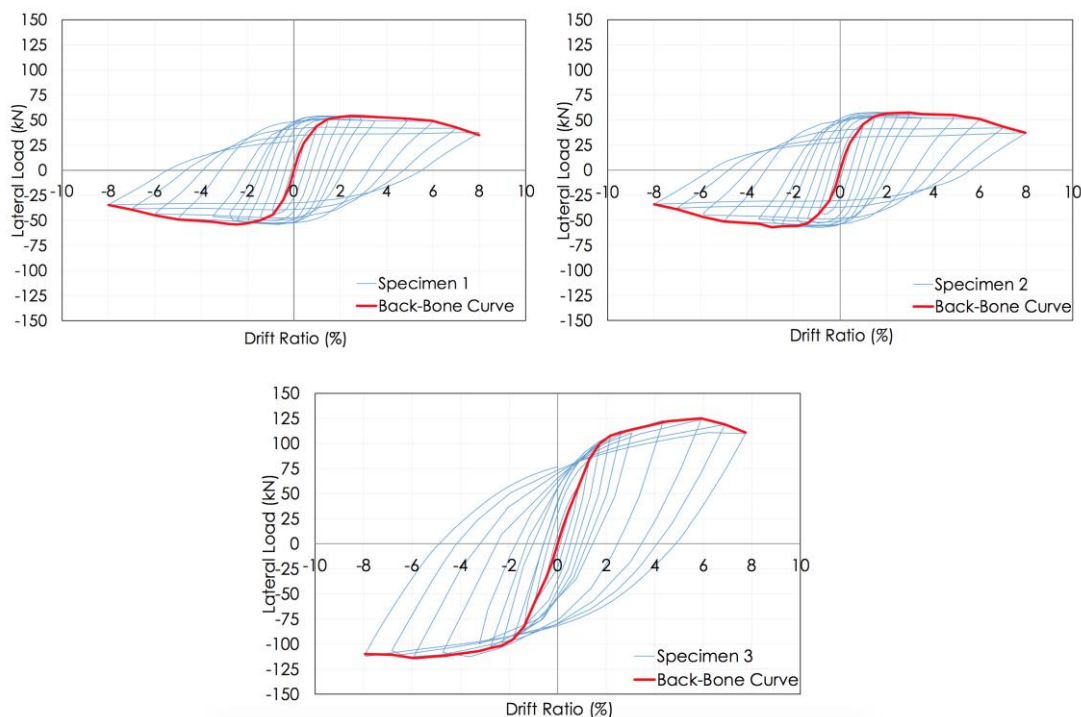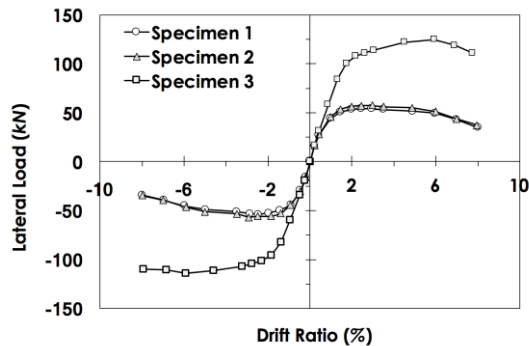

Figure 8 Hysteresis curves of all specimens

Table 2 Improvement of peak lateral load

Specimen	Peak Lateral Load (kN)			Ratio of Peak Lateral Load to Specimen Control (%)		
	Positive	Negative	Average	Positive	Negative	Average
1	54.20	54.06	54.13	100.00	100.00	100.00
2	57.48	56.98	57.23	106.05	105.40	105.72
3	125.00	114.00	119.50	230.62	210.87	220.74

Figure 9 Backbone curves of all specimens

3.3 Strength Degradation

Strength degradation is measured by a ratio of lateral force under targeted drift ratio to the maximum lateral force. According to ACI Committee [22], the strength ratio should not less than 75% for both of the loading directions at the allowable drift ratio of 3.5%.

As presented in Table 3, specimen 3 shows the superior performance related to the strength degradation. Under targeted drift ratio up to 8.0%, the lateral force of specimen 3 is still greater than that of required strength degradation of 75%. On the contrary, both of the specimens 1 and 2 do not satisfy the required strength degradation at the drift ratio of 8.0%. However, the strength degradation of specimen 1 and 2 at the drift ratio of 3.5% still qualifies the required ratio of stiffness degradation whereby the results indicate that at the drift ratio of 3.5%, specimen 1 and 2 exhibited of more than 75% of average strength degradation. As a matter of fact, it can certainly be stated that the used of drop panel provides an insignificant strength degradation of slab-column connection.

Table 3 The feasibility of strength degradation of all specimens

Specimen	Maximum Lateral Force (kN)			Lateral Forces under Targeted Drift Ratio (kN)			Ratio of Strength Degradation (%)		
	Drift Ratio (%)	Positive Direction	Negative Direction	Drift Ratio (%)	Positive Direction	Negative Direction	Positive Direction	Negative Direction	Average
1	2.44	54.20	54.06	3.50	53.15	51.40	98.06	95.07	96.57
2	2.98	57.48	56.98	3.50	55.98	53.50	97.39	93.89	95.64
3	5.93	125.00	114.00	3.50	116.74	111.79	93.39	98.06	95.73
1	2.44	54.20	54.06	8.00	35.00	34.60	64.57	64.01	64.29
2	2.98	57.48	56.98	8.00	37.26	34.10	64.83	59.85	62.34
3	5.93	125.00	114.00	8.00	110.89	110.00	88.72	96.49	92.60

3.4 Adequacy of Initial Stiffness

The evaluation of the initial stiffness [22] is one of the requirements that must be complied in order to give a better response of structure due to the minor earthquake. The structure is assumed to possess the adequate initial stiffness if the nominal strength is achieved before drift exceeds an initial drift limit (*IDL*). In this case, the adequacy of initial stiffness is defined as the resultant of total bending moments in the slab (M_{total}) representing the lateral resistance under *IDL* must surpass the nominal bending moments (M_n), or it can simply be said as the ratio of M_{total} to M_n which must exceed 100%.

In this study, the investigation of initial stiffness was also performed for each risk category. By using data from Figure 8, the value of initial stiffness can be obtained. Table 4 shows the ratio of the adequacy of initial stiffness of each specimen. From this table, it can be said that all specimens have fulfilled the requirement of initial stiffness designed for all risk category.

Table 4 Adequacy of initial stiffness

Risk Category	IDL	Ratio of M_{total}/M_n (%) for Each Specimen		
		1	2	3
I/II	0.40	150.90	153.34	167.88
III	0.30	138.88	141.08	151.79
IV	0.20	124.26	126.27	133.68

3.5 Stiffness Degradation

The sufficient stiffness degradation is needed to prevent the progressive collapse of the structure under major earthquake. While structures experience damage condition, it is highly suggested that structure must have integrity i.e. proper stiffness degradation to prevent sudden collapse. In this study, evaluation of stiffness degradation of each specimen was carried out based on the provision [22]. The initial stiffness K_0 is defined as the stiffness of the first cycle under drift ratio of 0.05%. The stiffness degradation is expressed as the ratio of initial stiffness and the stiffness under targeted drift ratio or must be greater than drift ratio of 3.5% with a minimum value of 5%. As the results of analysis, the evaluation of stiffness degradation of each specimen is tabulated in Table 5. From Table 5, it proves that all specimens qualify the requirement of provision [22]. The ratio of strength degradation in the loading phase at the drift ratio of 3.5% is greater than 5%.

Table 5 Feasibility of the stiffness degradation ratio

| Specimen	Positive Direction			Negative Direction		
	K_0	K'	K'/K_0	K_0	K'	K'/K_0 (%)
	(kN/mm)		(%)	(kN/mm)		(%)
1	5.47	0.97	17.68	8.59	0.94	10.90
2	5.49	1.02	18.57	8.54	0.97	11.40
3	8.10	2.12	26.23	7.54	2.03	26.98

3.6 Energy Dissipation

To assure that structure has an adequate hysteresis damping, the relative energy dissipation ratio, which is measured as the ratio of the third cycle at the drift ratio of 3.5% to the energy of the elastoplastic model, must not be less than 12.5%. The relative energy dissipation as shown in Table 6 is calculated as the hysteretic energy of the third cycle of hysteresis loop divided by the energy under the total area of hysteresis loop at the drift ratio of 3.5%. Table 6 shows that all specimens have the adequate energy dissipation up to drift ratio of 3.5%. It indicates that all specimens satisfy the requirement.

The energy dissipation also tends to increase under larger drift ratio, related to the plasticity occurred under large displacement. Figure 10 shows that energy dissipation of specimen 3 inclines to be larger than that of specimen 1 and 2 up to drift ratio of 3.5%. It proves that PVA fibers worked very well to dissipate the amount of energy due to cyclic service load.

Table 6 Evaluation of the stiffness degradation ratio

Specimen	E-3.5%	E-par	Relative Ratio of Energy Dissipation (%)
	(10^6 N-mm)		
1	2.91	8.64	33.65
2	3.08	8.33	36.97
3	4.82	8.12	59.41
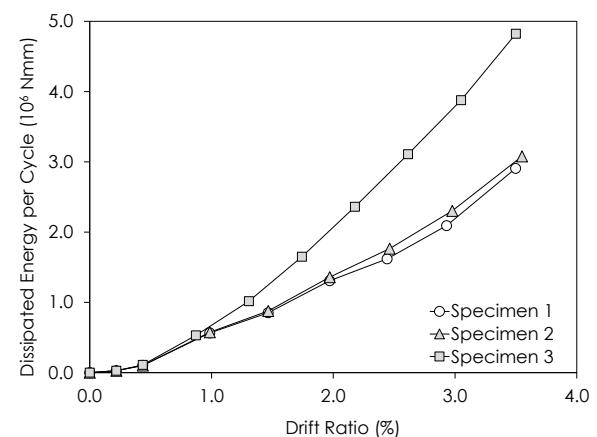
Figure 10 Energy dissipation up to drift ratio of 3.5%

3.7 Damage Contours

Crack patterns of specimen model can be visualized in ABAQUS. Cracking phenomenon of the structure occurs due to the concentration of stress at the particular location during the loading phase. In this study, the effect of reversed loading of cyclic lateral load affected the cracking behavior at the critical perimeter of slab-column connection. Figure 11 shows the typical post-cracking behavior of each specimen at the peak lateral load.

It is shown that specimen 1 and 2 have exhibited a quite similar trend of peak lateral load. This might occur due to the concrete element in the column being recessive and has achieved the nominal concrete strain thereby provoking the structure to exhibit unstable response. It can be seen from the contour that the stress concentration occurs in the intersection line between column face and slab. Although having such similar results, it is still shown that the post-cracking response around the slab in specimen 2 is way better than specimen S2 where there is no indication of the prominent crack

formation around the critical section compared to that specimen S1.

Another aspect that is encountered, specimen 3 performed the superior improvement up to drift ratio of 8%. The post-cracking contours show that even in the ultimate drift ratio, the value of maximum principle plastic strain is insignificant. One of the underlying reasons is caused by the used of PVA-ECC

material that is designed through micromechanics principle, hence the phenomenon of multiple micro-cracking is taken into consideration as the ability to prevent the structure against sudden collapse. Overall, it can be well-said that PVA-ECC was run in the appropriate behavior to sustain the combined gravity and cyclic lateral loads.
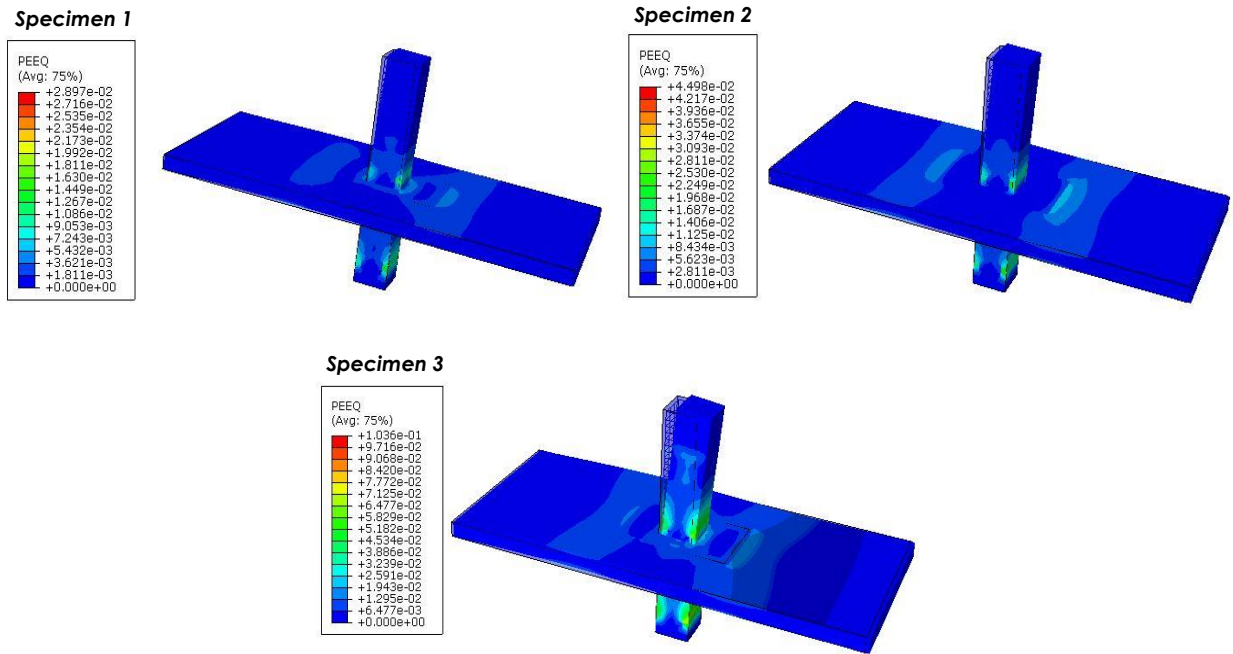

Figure 11 Crack patterns of all specimens at peak lateral load

4.0 CONCLUSION

Based on the results of numerical simulation as presented above, several conclusions are drawn.
1) In general, specimen 3 represents the most qualified model to be applied in construction field due to its impressive behavior related to strength, stiffness, lateral capacity, and energy dissipation when being subjected to combined gravity load and cyclic lateral load.
2) The larger initial stiffness and better stiffness degradation ratio of specimen 3 indicates that PVA-ECC material not only improves the stiffness but also undergoes the significant stiffness degradation.
3) Considering the adequacy of strength degradation, specimen 3 does not experience degradation in strength at drift ratio 3.5%, while specimen 1 and 2 suffer such degradation. However, up to this drift cycle, specimen 1 and 2 still satisfiy the minimum requirement specified in ACI.
4) In terms of lateral load capacity, specimen 2 displayed a slightly higher load capacity than specimen 1, while specimen 3 shows the significant increase of lateral load capacity.

Although the results seem to be promising, however,, this study was only carried out with the support of FE software. Thus, to assure the accuracy of this study, the experimental test must be then performed as the verification variable for the FE analysis.

Acknowledgement

The first author wishes to acknowledge the Ministry of Research, Technology and Higher Education of the Republic of Indonesia, for PMDSU scholarship that enabled him to carry out this work.

References

[1]   Robertson, I. N., Kawai, T., Lee, J., and Enomoto, B. 2000. Cyclic Testing of Slab-Column Connections with Shear Reinforcement. *ACI Structural Journal*. 99(5): 605-613.
[2]   Gunadi, R., Budiono, B., Imran, I., and Sofwan, A. 2014. The Behavior of Slab-Column Connections with Modified Shear Reinforcement under Cyclic Load. *Journal of Engineering and Technological Sciences – ITB.* 46(1): 17-36.
[3]   Qian, K. and Li, B. 2013. Experimental Study of Drop-Panel Effects on Response of Reinforced Concrete Flat Slabs after Loss of Corner Column. *ACI Structural Journal*. 110(2): 319-330.

[4] Hueste, M. B. D., Browning, J., Lapage, A., and Wallace, J. W. 2007. Seismic Design Criteria for Slab-Column Connections. *ACI Structural Journal*. 104(4): 448-458.

[5] King, S. and Dallate, N. J. 2004. Collapse of 2000 Commonwealth Avenue: Punching Shear Case Study. *Journal of Performance of Constructed Facilities–ASCE*. 18(1): 54-61.

[6] Park, T. W. 2011. Inspection of Collapse Cause of Sempoong Department Store. *Forensic Science International*. 217(1-3): 119-126.

[7] Megally, S., and Ghali, A. 2000. Punching Shear Design of Earthquake-Resistant Slab-Column Connections. *ACI Structural Journal*. 97(5): 720-730.

[8] Graf, W. P. and Mehrain, M. 1992. Analysis and Testing of a Flat Slab Concrete Building. *Earthquake Engineering, Tenth World Conference, Balkema. Rotterdam*. 3387-3392.

[9] Kang, T. H. K., Wallace, J. W., and Elwood, K. J. 2006. Dynamic Tests and Modeling of RC and PT Slab-Column Connections. *Proceedings of the 8th U.S. National Conference on Earthquake Engineering*. San Francisco, California.

[10] McHarg, P. J., Cook, W. D., Mitchell, D., and Yoon, Y. S. 2000. Benefits of Concentrated Slab Reinforcement and Steel Fibers on Performance of Slab-Column Connections. *ACI Structural Journal*. 97(2): 225-235.

[11] Sahmaran, M., and Li, V. C. 2008. Durability of Mechanically Loaded Engineered Cementitious Composites under Highly Alkaline Environments. *Journal of Cement and Based Composites*. 30(2): 72-81.

[12] Roth, M. J. 2008. Flexural and Tensile Properties of Thin, Very High-Strength, Fiber-Reinforced Concrete Panels. *Modular Protective Systems for Future Force Assets*. Vicksburg: U.S. Army Engineer Research and Development Center.

[13] Li, V. C., Kim, J. K., Kim, Y. Y. 2010. Prediction of ECC Tensile Stress-Strain Curve Based on Modified Fiber Bridging Relations Considering Fiber Distribution Characteristic. *Computer and Concrete*. 7(5): 455-468.

[14] Gunadi, R., Budiono, B., Imran, I., and Sofwan, A. 2012. Peningkatan Perilaku Hubungan Pelat-Kolom Terhadap Beban Lateral Siklis Dengan Menggunakan Detail Tulangan Geser Baru. *Prosiding Konferensi Nasional Pascasarjana Teknik Sipil (KNPTS)*. Bandung, Indonesia. 66-76.

[15] ACI – ASCE Committee 352. 2004. Recommendations for Design of Slab-Column Connections in Monolithic Reinforced Concrete Structures. *American Concrete Institute*. ACI 352.1R-89.

[16] ACI – ASCE Committee 421. 2008. Guide to Shear Reinforcement for Slabs. *American Concrete Institute*. ACI 421.1R-08.

[17] European Committee for Standardization (CEN). 2004. EN 1992-1-1: Eurocode 2: Design of Concrete Structures – Part 1-1: *General Rules and Rules for Buildings*.

[18] Kmiecik, P., and Kaminski, M. 2011. Modelling of Reinforced Concrete Structures and Composite Structures with Concrete Strength Degradation Taken into Consideration. *Archives of Civil and Mechanical Engineering*. 11(3): 623-636.

[19] Pavlovic, M., Markovic, Z., Veljkovic, M., and Budevac, D. 2013. Bolted Shear Connectors Vs. Headed Studs Behaviour in Push-Out Tests. *Journal of Constructional Steel Research – ELSEVIER*. 88: 134-149.

[20] Wang T., and Hsu, T. T. C. 2001. Nonlinear Finite Element Analysis of Concrete Structures Using New Constitutive Models. *Computer and Structures*. 79: 2781-2791.

[21] ABAQUS User Manual Version 6.10. 2014. *SIMULIA Corp.*

[22] ACI Committee 374. 2005. Acceptance Criteria for Moment Frames Based on Structural Testing and Commentary. *American Concrete Institute*. ACI 374.1-05.

[23] Hemati, A., Kheyroddin, A., and Sharbatdar, M.K. 2015. Plastic Hinge Rotation Capacity for Reinforced HPFRCC Beams. Journal of Structural Engineering – ASCE. 141(2): 1-11.